Supporting Information

Ligand-Induced Morphological Engineering and Electronic Modulation of CoCu Bimetallic Catalysts for Efficient HMF Electrooxidation

Hua Yu[a], Li Xu[a], Guizhen Li[b], Wei Xu[b], Yuxin Wang[a], Wen Zhang*[a]

[a] State Key Laboratory of Chemical Engineering and Low-Carbon Technology, Tianjin Key Laboratory of Membrane Science & Desalination Technology, and School of Chemical Engineering and Technology, Tianjin University, Tianjin 300350, China

[b] Tianjin Mainland Hydrogen Equipment Co., Ltd., Tianjin, 301609, China

*Corresponding author E-mail: zhang_wen@tju.edu.cn

1 Chemicals and materials

Cobalt(II) nitrate hexahydrate ($Co(NO_3)_2·6H_2O$, 99%) and copper(II) nitrate trihydrate ($Cu(NO_3)_2·3H_2O$, 99%) ammonium formate (chromatography grade, ≥99.9%), and formic acid (HPLC grade) were purchased from Shanghai Aladdin Reagent Co., Ltd. Potassium hydroxide (KOH, GR grade, 85%) and methanol (HPLC grade, 99%) were purchased from Tianjin Kemiou Reagent Co., Ltd. 2,6-naphthalenedicarboxylic acid (2,6-NDA, 98%) were purchased from Tianjin Heowns Biochemical Technology Co., Ltd. Potassium 2,6-naphthalenedicarboxylate (2,6-K_2NDA, 97%) were purchased from Shanghai Bide Pharmaceutical Technology Co., Ltd. 5-Hydroxymethylfurfural (HMF, 97%) and 2,5-furanedicarboxylic acid (FDCA, 99.5%) were purchased from Adamas Limited. 5-Hydroxymethylfurfural carboxylic acid (HMFCA, 98%) and 5-Formyl-2-furancarboxylic acid (FFCA, 99.9%) were purchased from Alpha Aesar. 2,5-diformylfuran (DFF, 98%) were purchased from Shanghai Aladdin Reagent Co., Ltd. Anhydrous ethanol was purchased from Tianjin Aopusheng Chemical Co., Ltd. The resistivity of ultrapure water was 18.25 MΩ·cm. All chemical reagents were used directly without further purification. Additionally, Nickle foam (NF) used in the experiments was procured from Tianjin Liweitan Technology Co., Ltd.

2 Characterization

The crystal structure was characterized using X-ray diffraction (XRD, Bruker D8-Focus, Cu-Kα radiation at 40 kV, λ=1.5418 Å) with a scan range of 5°-70° and a scan rate of 5° min^{-1}. Fourier transform infrared (FT-IR) spectra were recorded on a Gangdong FTS-650 spectrometer to investigate the coordination structure of the catalysts. The samples were prepared using the KBr pellet method under a pressure of 10 MPa for 60 seconds. The spectra were collected with 32 scans at a resolution of 4 cm^{-1}. Electrode samples were tested using a confocal Raman spectrometer (HORIBA LabRAM HR Evolution, excitation wavelength: 532 nm, acquisition time: 10 s). Morphological observation of the prepared samples was performed using a scanning electron microscope (SEM, Hitachi 8100, Japan). Transmission electron microscopy (TEM) and high-resolution TEM images were obtained using a transmission electron microscope (JEOL JEM-2100F, Japan) equipped with an energy-dispersive spectrometer (EDS). Electrode samples were analyzed using an X-ray photoelectron spectrometer (Thermo Scientific ESCALAB 250XI, X-ray source: Al Kα (energy 1486.68 eV), acceleration voltage 15 kV). Notably, the vacuum level in the analysis chamber was maintained at $<10\times10^{-8}$ mbar. XPS data peak fitting was performed using XPSPEAK41 software.

3 Product quantification

The concentration of organic compounds was determined using high-performance liquid chromatography (HPLC, LC-20AD, Shimadzu) equipped with a UV-visible detector set at 265 nm and a C18 column. Mobile phase A: 1045 g DI water + 1.76 g ammonium formate + 1 mL formic acid + 43.5 g methanol, flow rate 0.425 mL min^{-1}; Mobile phase: Phase B: methanol, flow rate 0.075 mL min^{-1}. Column temperature was set at 60°C. For each analysis, 100 μL of anodic electrolyte was diluted to 3 mL with 0.2 mol/L sulfuric acid. Subsequently, 1 mL of this mixture was taken and combined with 350 μL 1 mol/L KOH + 650 μL DI water. Each run lasted 20 minutes. Product quantification was performed using the external standard method. The conversion rate of HMF ($\mathrm{Conv.}_{\mathrm{HMF}}$), the yield of FDCA ($\mathrm{Yield}_{\mathrm{FDCA}}$), and the Faraday efficiency (FE) were calculated according to the following equations:

$$Conversion\ (\%) = \frac{mole\ of\ consumed\ HMF}{mole\ of\ initial\ HMF} \times 100\%$$

$$Yield\ (\%) = \frac{mole\ of\ formed\ FDCA}{mole\ of\ consumed\ HMF} \times 100\%$$

$$Faradaic\ efficiency\ (\%) = \frac{mole\ of\ formed\ FDCA}{Q} \times 6 \times F \times 100\%$$

Q is the charge transferred over the reaction, and F is the Faraday constant (96485 C mol^{-1}).

The carbon balance was calculated according to the following equation:

$$Carbon\ balance\ (\%) \ = \frac{n_{HMF} + n_{\mathrm{HMFCA}} + n_{\mathrm{DFF}} + n_{\mathrm{FFCA}} + n_{\mathrm{FDCA}}}{mole\ of\ initial\ HMF} \times 100\%$$

where n represents the mole of each species.

4 Supplementary figures and tables

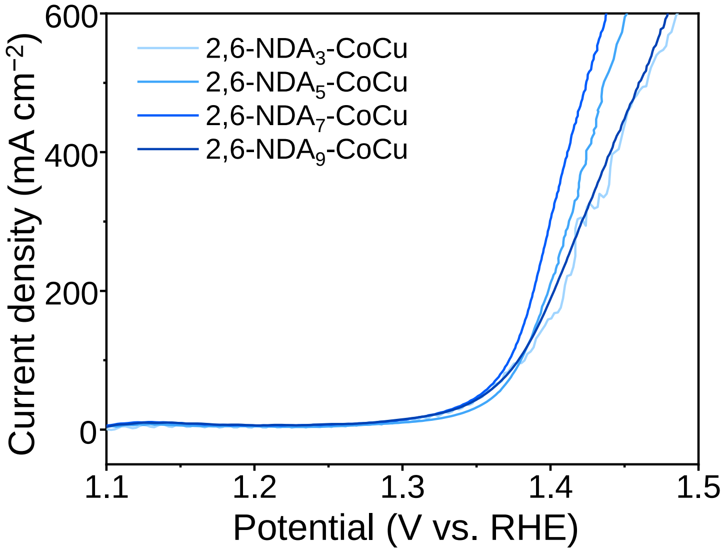

Fig. S1 The 2,6-NDA$_x$-CoCu catalyst synthesized by electrodeposition with varying molar ratios of 2,6-NDA (x=3,5,7,9).

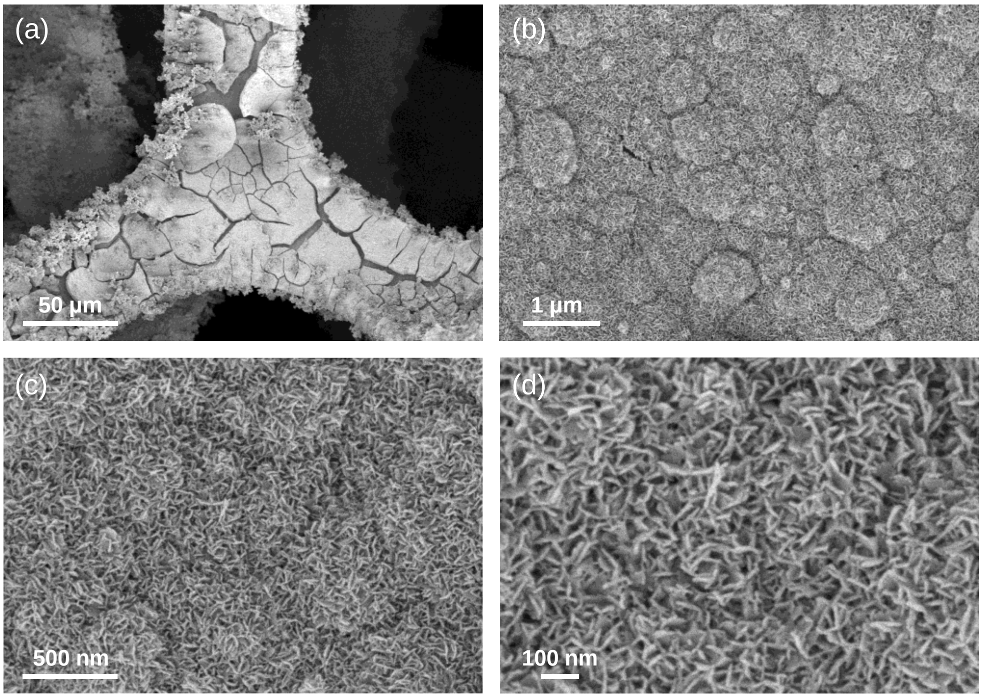

Fig. S2 (a-d) The SEM images of CoCu at different magnifications.

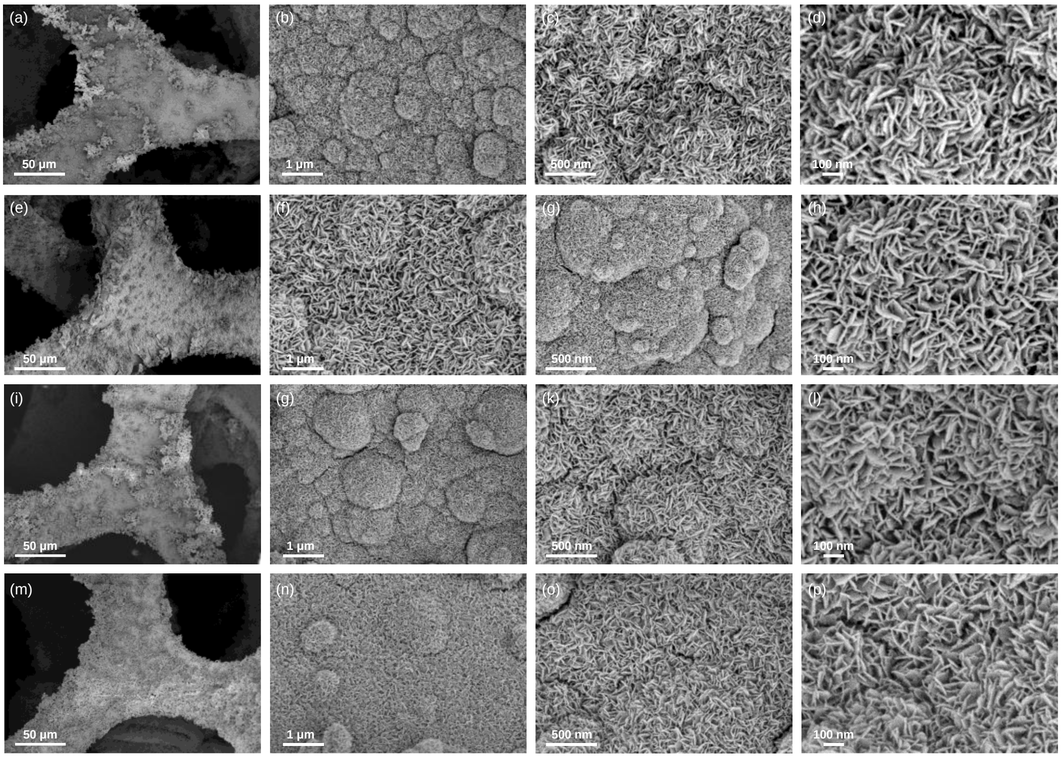

Fig. S3 (a-d) 2,6-NDA$_3$-CoCu , (e-h) 2,6-NDA$_5$-CoCu, (e-h) 2,6-NDA$_7$-CoCu and (e-h) 2,6-NDA$_9$-CoCu at different magnifications.

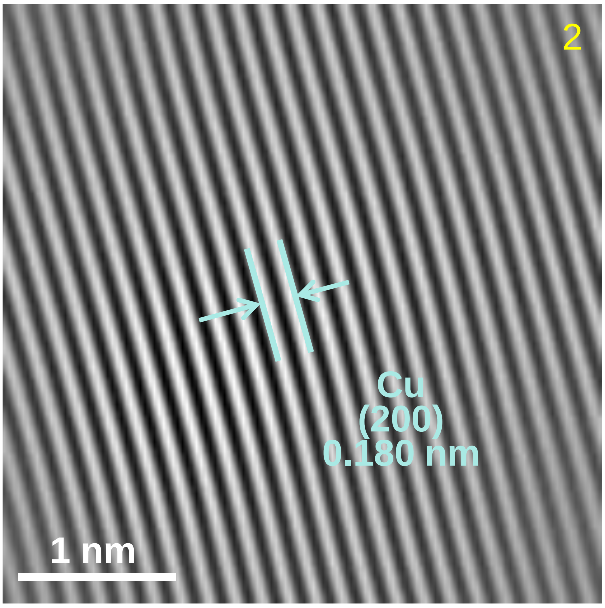

Fig. S4 The corresponding IFFT filtered image of the region marked by the white square 2.

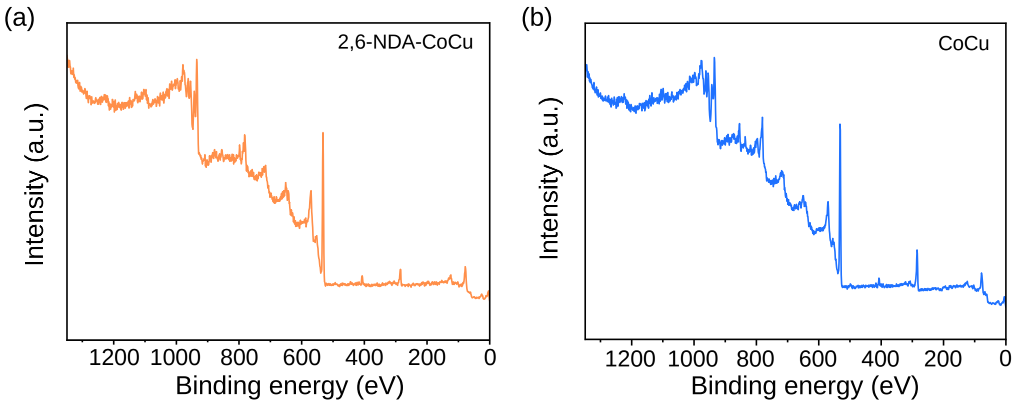

Fig. S5 The full scan XPS spectra of (a) 2,6-NDA-CoCu and (b) CoCu.

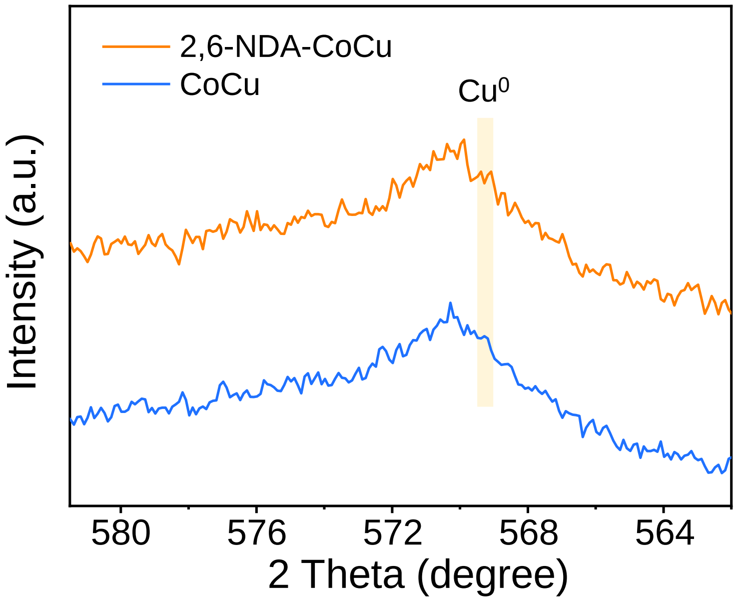

Fig. S6 Cu LMM Auger spectra of 2,6-NDA-CoCu and CoCu.

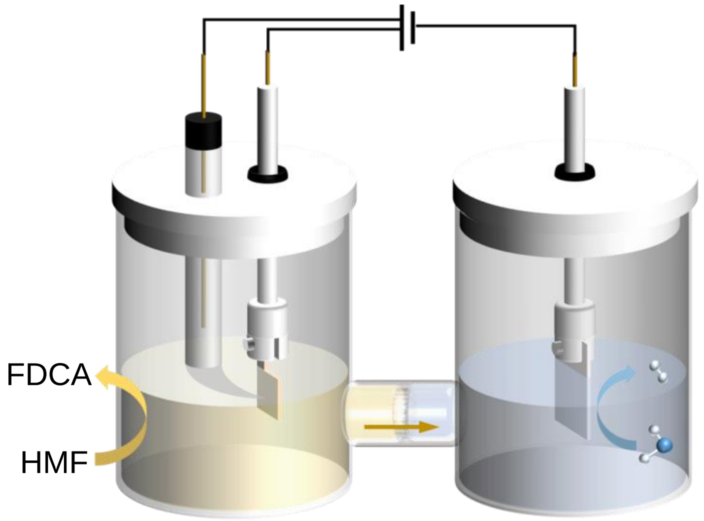

Fig. S7 Electrochemical system for the electrooxidation of HMF.

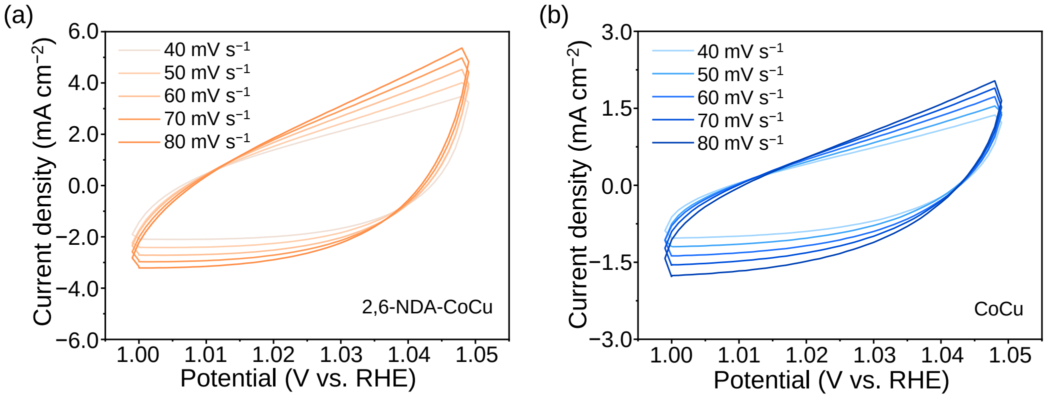

Fig. S8 The CV curves of (a) 2,6-NDA-CoCu and (b) CoCu 1 mol/L KOH and 50 mmol/L HMF with various scan rates (40/50/60/70/80mV s^{-1}).

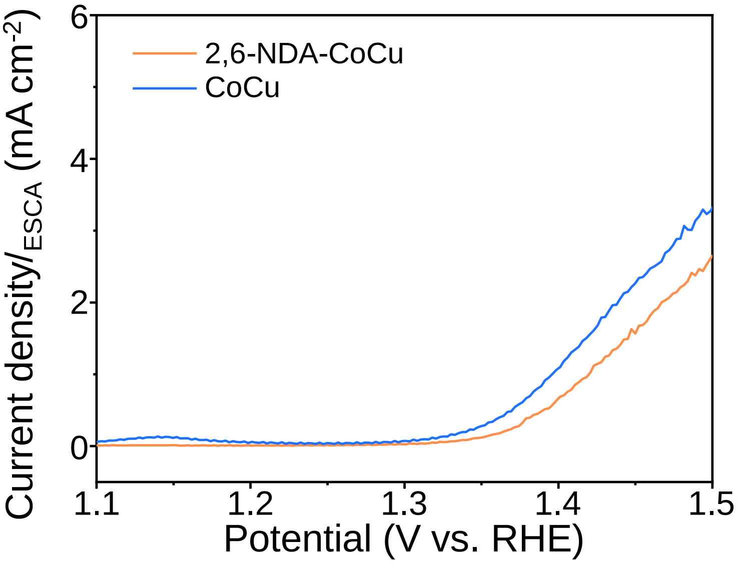

Fig. S9 ECSA-normalized LSV curve.

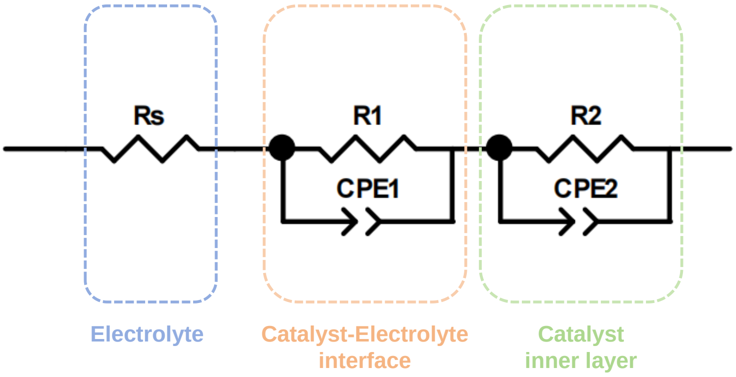

Fig. S10 Equivalent circuit model containing electrolyte and electrolyte-catalyst.

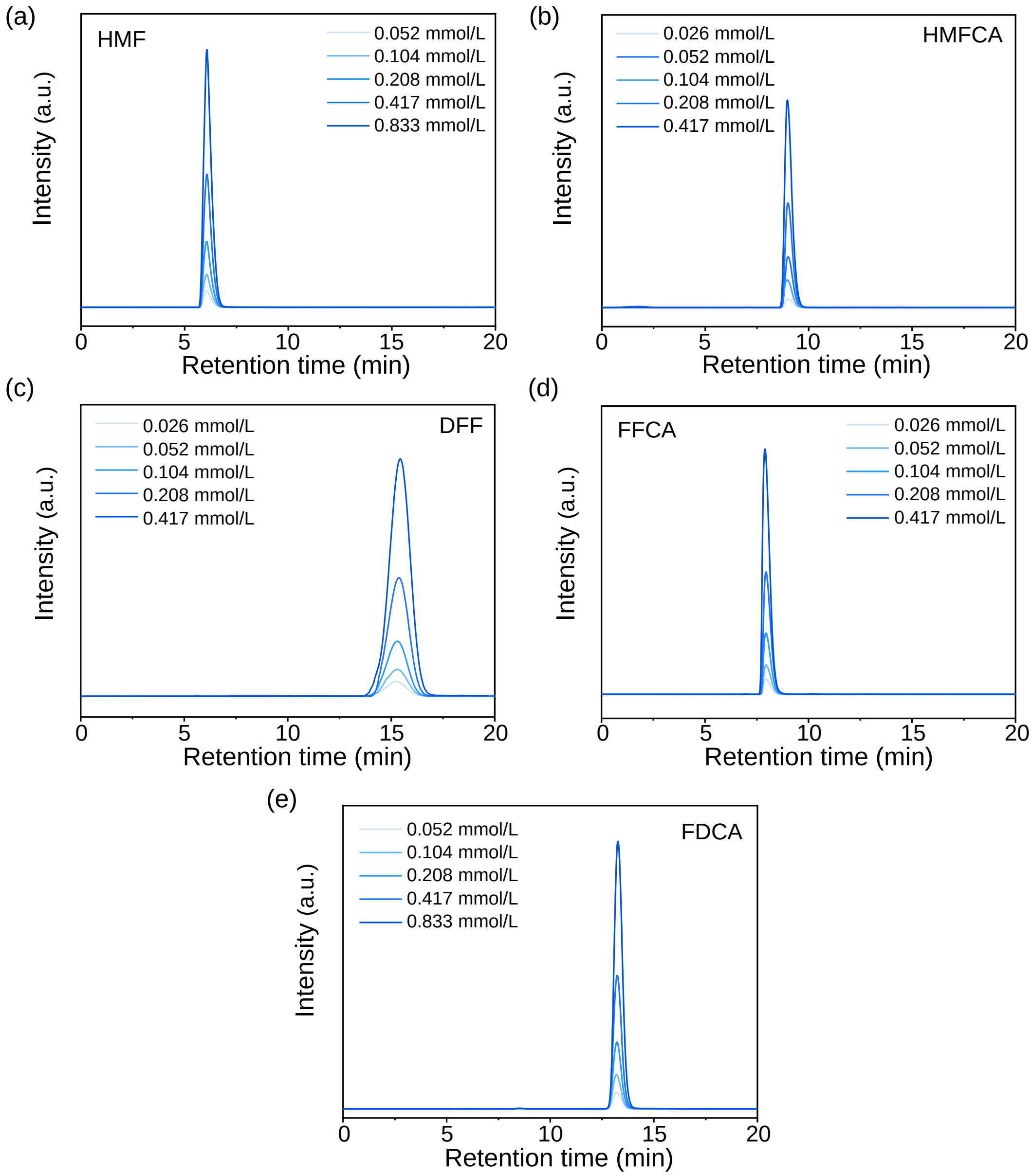

Fig. S11 The elution curve of related standard mixtures of (a) HMF, (b) HMFCA, (c) DFF, (d) FFCA and (e) FDCA with different concentrations.

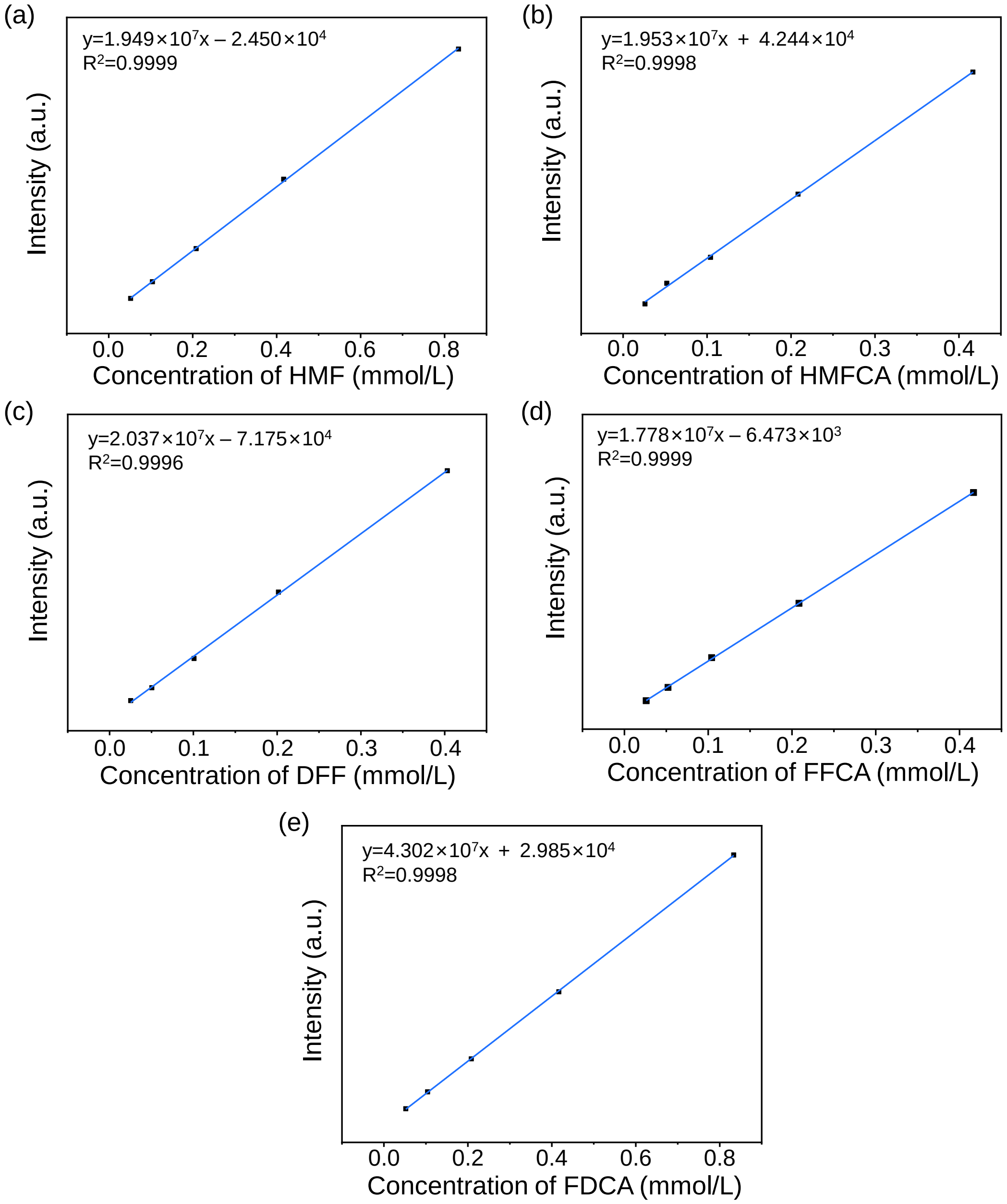

Fig. S12 HPLC analysis. HPLC chromatograms and corresponding standard curves for (a) HMF, (b) HMFCA, (c) DFF, (d) FFCA and (e) FDCA with different concentrations.

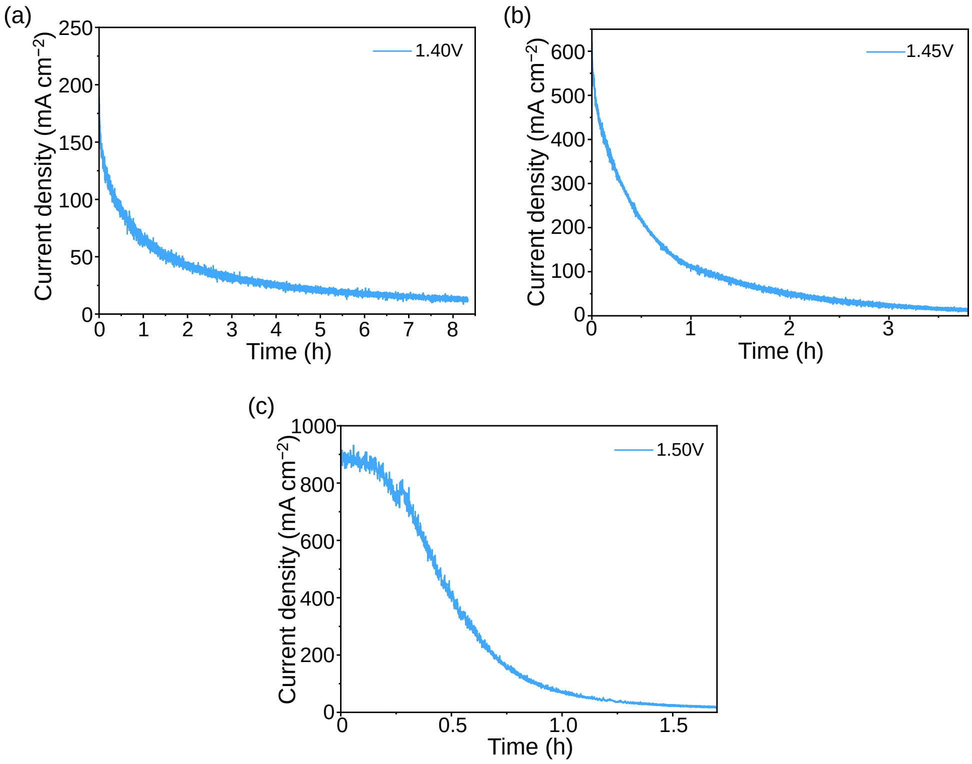

Fig. S13 Chronoamperometric curves of 2,6-NDA-CoCu at in (a) 1.40 V, (b) 1.45 V and (c) 1.50 V in 1 mol/L KOH with 50 mmol/L HMF.

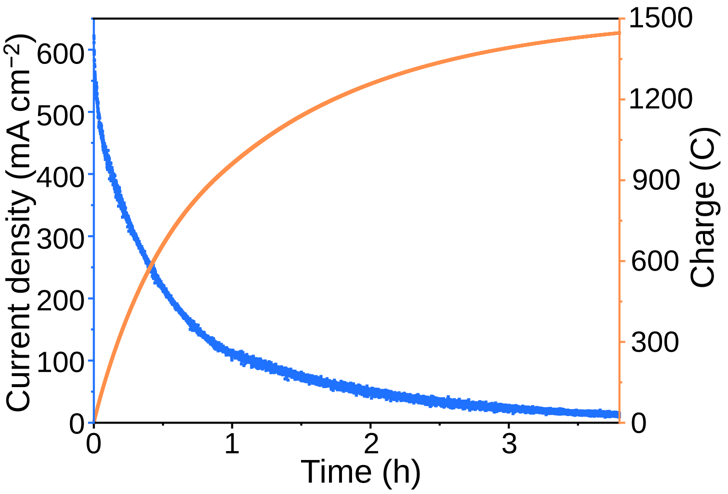

Fig. S14 Chronoamperometric curves and passed charge of 2,6-NDA-CoCu at 1.45V with 50 mmol/L HMF in 1 mol/L KOH solution.

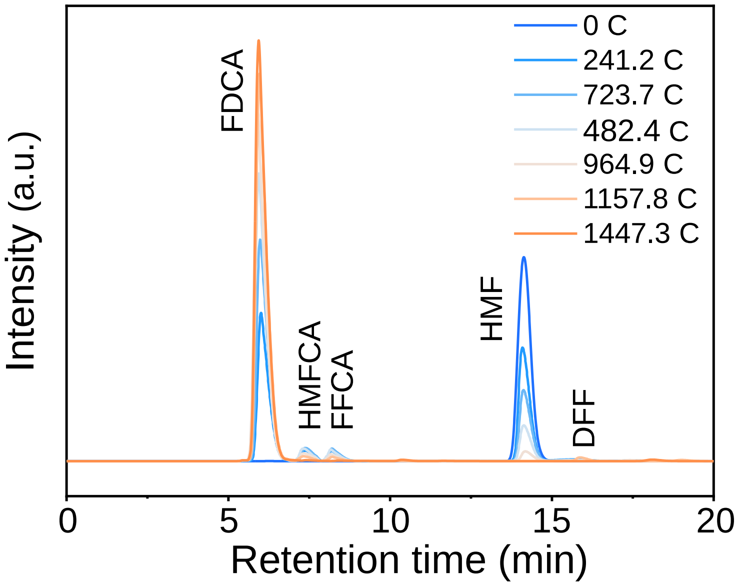

Fig. S15 HPLC chromatogram of the electrolyte at various electrolysis charges.

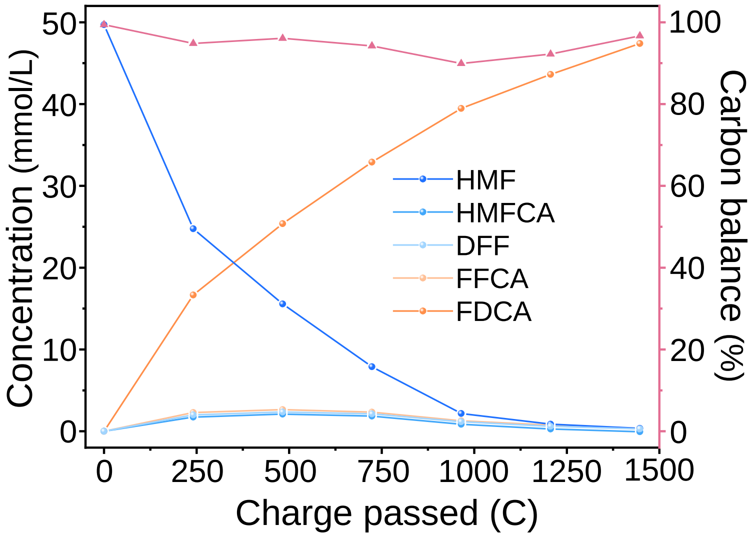

Fig. S16 Evolution of organic matter concentrations as a function of charge input and the corresponding carbon balance.

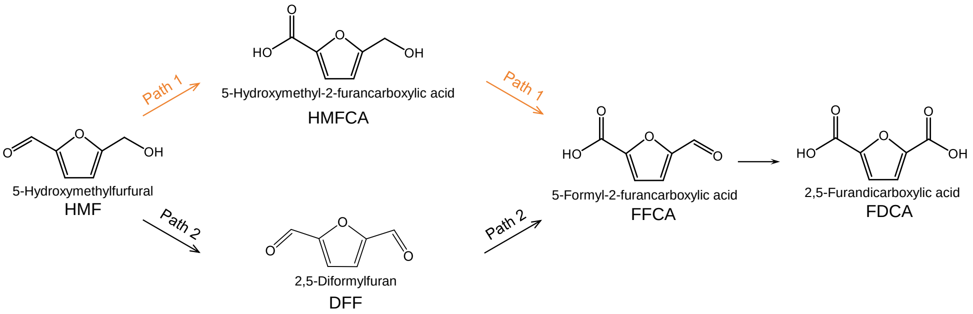

Fig. S17 Schematic reaction process HMFOR.

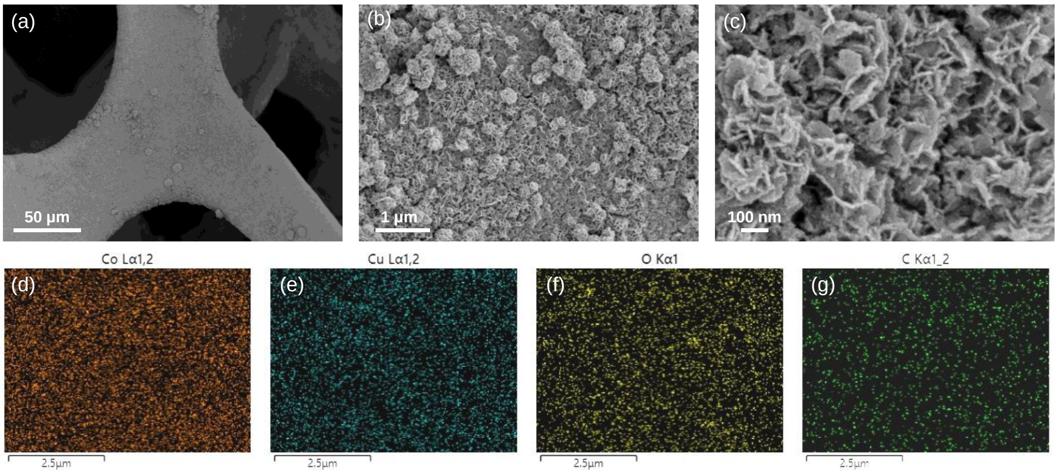

Fig. S18 (a-c) The SEM images and (d-g) EDS elemental maps of 2,6-NDA-CoCu after 10 consecutive HMFOR cycles at different magnifications.

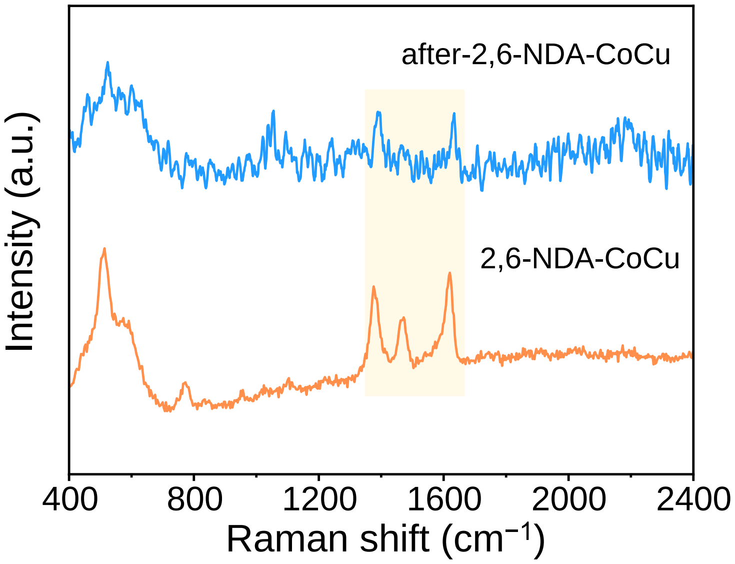

Fig. S19 Raman spectra of 2,6-NDA-CoCu before and after 10 consecutive electrolysis cycles.

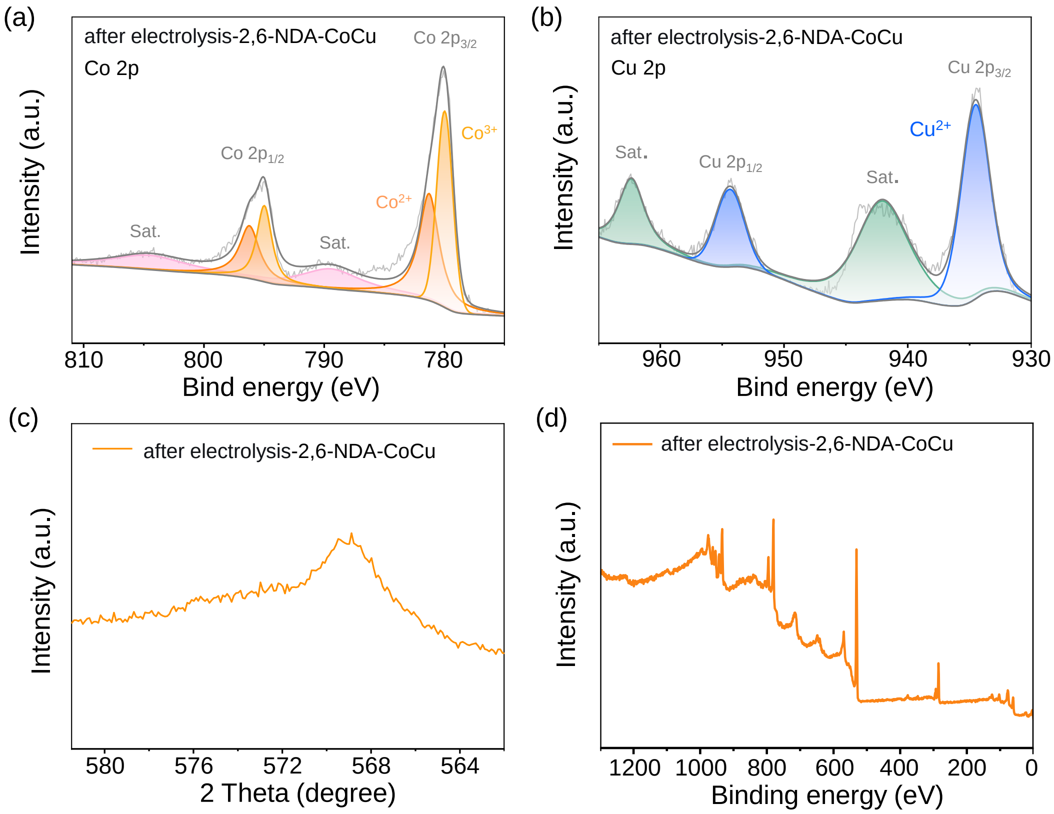

Fig. 20 XPS characterization of the 2,6-NDA-CoCu electrode after ten electrolysis cycles: (a) high-resolution Co 2p XPS spectrum, (b) high-resolution Cu 2p XPS spectrum, (c) Cu LMM Auger spectrum, and (d) survey XPS spectrum.

Note: The Co 2p XPS spectrum shows that the post-electrolysis sample exhibits characteristic Co $2p_{3/2}$ peaks for Co^{3+} and Co^{2+} at 779.98 eV and 781.46 eV, respectively, and Co $2p_{1/2}$ characteristic peaks for Co^{3+} and Co^{2+} at 796.25 eV and 804.36 eV, respectively. This confirms that Co exists as a mixed valence state (Co^{2+}/Co^{3+}) after the reaction, and that high-valence Co^{3+} is retained during the reaction. Combined with the electrochemical performance, we identify high-valence Co^{3+} as the genuine active site for the HMFOR process.

The Cu 2p XPS spectrum reveals that the characteristic peak of Cu^0 completely disappears after electrolysis, while new peaks assigned to Cu^{2+} appear at 934.55 eV (Cu $2p_{3/2}$) and 954.39 eV (Cu $2p_{1/2}$). In addition, no clear Cu^0 signal is observed in the Cu LMM Auger spectrum, indicating that Cu^0 is completely converted to Cu^{2+}. This does not conflict with the presence of Cu^0 in the as-synthesized pre-catalyst. During the activation process, the 2,6-NDA-CoCu pre-catalyst undergoes in situ reconstruction under anodic potential to form Cu^{2+}.[1,2]

Regarding the role of the activated Cu^{2+}, previous studies have shown that in situ generated Cu^{2+} species can stabilize high-valence Co^{3+} through electronic interactions, and also improve the conductivity of the electrode interface and hydroxyl adsorption capacity.[1,3,4] To further validate the contribution of Cu, we compared the LSV performance of a Cu-free control sample, 2,6-NDA-Co, with that of 2,6-NDA-CoCu (Fig. S21). The results show that 2,6-NDA-CoCu exhibits superior catalytic activity to 2,6-NDA-Co, indicating that even though Cu^0 is converted to Cu^{2+} during the reaction, the presence of Cu remains indispensable for enhancing the overall catalytic performance.

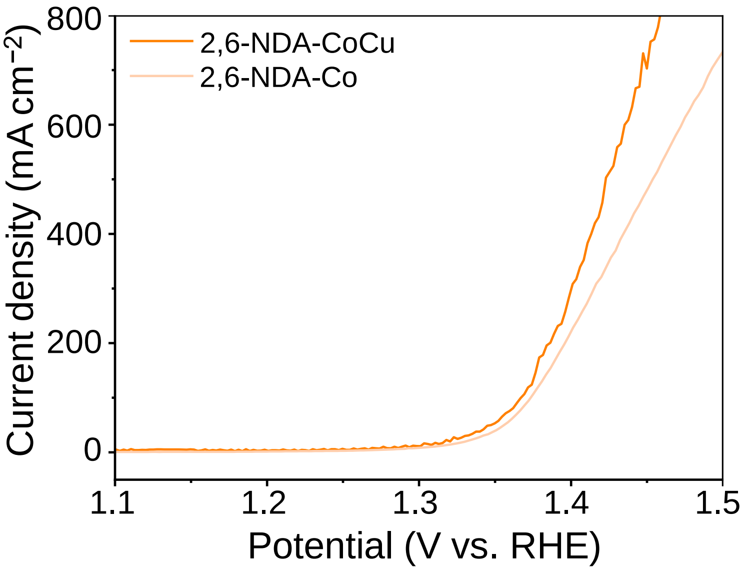

Fig. S21 Comparison of LSV curves for HMFOR on 2,6-NDA-CoCu and 2,6-NDA-Co.

5 References

1 P. Zhao, B. Chen, W. Zhao, Z. Chen, L. Guan, Y. Li, W. Peng, J. Zhang, Q. Zhang and X. Fan, *ACS Catal.*, 2025, **15**, 15132–15140.

2 G. Tong, K. Zheng, Z. Feng, R. Su, X. Liu, X. Tao, C. Zhang and C. Xu, *Angew. Chem. Int. Ed.*, 2025, **64**, e202512175.

3 S. Liu, S. Dou, J. Meng, Y. Liu, Y. Liu and H. Yu, *Appl. Catal. B*, 2023, **331**, 122709.

4 X. Tao, G. Tong, C. Zhang, X. Liu, X. Meng, C. Xu and K. Zheng, *Appl. Surf. Sci.*, 2026, **726**, 165915.